

Article

Municipal Solid Waste Incineration Bottom Ash as Sole Precursor in the Alkali-Activated Binder Formulation

Àlex Maldonado-Alameda , Jessica Giro-Paloma , Anna Alfocea-Roig, Joan Formosa 
and Josep Maria Chimenos * 

Departament de Ciència de Materials i Química Física, Universitat de Barcelona, C/Martí i Franquès, 1, 08028 Barcelona, Spain; alex.maldonado@ub.edu (À.M.-A.); jessicagiro@ub.edu (J.G.-P.); annaalfocea@ub.edu (A.A.-R.); joanformosa@ub.edu (J.F.)

* Correspondence: chimenos@ub.edu; Tel.: +34-93-403-7244

Received: 16 May 2020; Accepted: 13 June 2020; Published: 16 June 2020



Abstract: The concern about the large amount of weathered bottom ash (WBA) produced in waste-to-energy plants (WtE) has caused an increased search for alternatives to reduce their environmental impact. The present study aims to provide an added value through the WBA valorization from municipal solid waste incineration (MSWI) for its use as a sole precursor for developing alkali-activated binders (AABs). Alkali-activated weathered bottom ash binders (AA-WBA) were formulated with a liquid-to-solid ratio of 1.0 and using sodium silicate (80 wt.%) and NaOH (20 wt.%) at different concentrations (2, 4, 6, and 8M) as alkali-activator solutions. AA-WBA were cured at room temperature to extend their applicability. The effect of the alkali-activator solution molarity on the final properties of the AA-WBA was evaluated. The physicochemical characterization by XRD, FTIR, and SEM evidenced the presence of the typical phases (calcium silicate hydrate and gehlenite) of C-(A)-S-H gel. Leaching concentrations of As, Cu, and Mo exceed the acceptance in landfills for inert waste, while the leaching concentration of Sb exceeds the one for non-hazardous waste. The structure of the binders depends on the alkalinity of the activator, obtaining better results using NaOH 6M in terms of microstructure and compressive strength (6.7 MPa). The present study revealed that AA-WBA for non-structural purposes can be obtained. The AA-WBA formulation contributes to the WBA valorization and development of low-carbon cements; therefore, it is an encouraged alternative to ordinary Portland cement (OPC). Considering the amounts and costs of the WBA, sodium silicate, NaOH, and water, the total cost of the developed formulations is comprised in a range between 137.6 and 153.9 €/Tn.

Keywords: waste recycling and management; valorization; weathered bottom ash; municipal solid waste incineration; alkali-activated binder

1. Introduction

Municipal solid waste incineration (MSWI) in waste-to-energy (WtE) plants is one of the main processes for municipal solid waste (MSW) management [1]. MSWI contributes to the energy recovery from MSW, and the reduction of its volume (by 90%) and weight (by 75%) [2]. It is extensively applied in many European countries. According to the information provided by the Confederation of European Waste-to-Energy Plants (CEWEP) [3], 492 WtE plants are operating in Europe [4]. In 2017, around 70 Mt of MSW were incinerated in the EU (EU-28) [5]. The main by-product produced during the MSW treatment in WtE plants is the incinerator bottom ash (IBA). IBA represents 85% of the solid resulting from combustion [6] and it is classified as a hazardous (EWC 19 01 11*—asterisk means hazardous) or non-hazardous waste (EWC 19 01 12) depending on its concentration of hazardous

substances. It is mainly composed of Si, Al, Ca, and Na oxides, and a small amount of heavy metal(loid)s [7]. IBA undergoes previous stabilization through an outdoor maturation treatment of 2–3 months, consisting of its carbonation and pH stabilization at values between 8–10 [8]. The resultant by-product of the IBA maturation treatment is weathered bottom ash (WBA), which is valorized for engineering purposes. The main application fields of WBA as secondary material are civil engineering, chemical engineering, and the building sector as reported elsewhere [9]. However, new applications of WBA have emerged in recent years for its use as a precursor on alkali-activated cements (AACs) [10] due to its composition rich in silicates and aluminosilicates [7].

AACs have become an alternative to ordinary Portland cement (OPC) given that the manufacturing process involves CO₂ reductions, energy-savings, and lower resource consumption. This fact has been certified by the large amount of studies published in the last decade [11,12]. Their obtention consists of the reaction of a solid powder precursor (based on amorphous aluminosilicates) [13] in an alkaline activate solution (usually NaOH, KOH, and/or Na₂SiO₃) of variable concentration. After a suitable activation process, a gel is formed (N-A-S-H, C-A-S-H, or N-(C)-A-S-H), of which the nature and final properties depend on the CaO content of the precursor [14], the alkali activator used [15], and the curing temperature [16]. AACs have good mechanical properties [17], high resistance to chemical attack by aggressive aqueous and acid solutions [18], and resistance to high temperatures and fire [19]. The carbon emission levels generated during AAC production are lower than that of OPC [20], which is beneficial from an environmental point of view. AACs are sustainable materials since these can be formulated from waste materials and industrial by-products [21,22]. Because of their similar properties to OPC, AAC applications are associated with building and civil engineering [23], as well as for the stabilization and solidification of hazardous and radioactive wastes [24–26]. For all of the above-mentioned reasons, AACs have shown a high potential to be applied as sustainable cements following the zero waste principle [27] promoted by EU [28].

Most of the published studies that include WBA in their AAC formulations add other precursors such as metakaolin [29], fly ash of thermal power plants [30], granulated blast furnace slag [31], or ladle slag [32] to obtain AACs. In all the cases described above, the reported AACs' strength values were low due to the presence of metallic Al found in WBA samples. Aluminum reacts with the alkali activator by forming hydrogen gas [33,34], increasing the porosity of AACs and decreasing the mechanical strength. On the other hand, great results were obtained when WBA was also used as a raw material in alkali-activated blended or hybrid cements to increase the AACs' mechanical strength [30,35–37]. There are few studies where WBA is used as a sole precursor [38–40]. However, the potential use of WBA as a sole precursor in AAC formulation was revealed by analyzing the SiO₂ and Al₂O₃ reactive phases through different chemical attacks [41]. AACs for non-structural purposes (compressive strength results were around 0.95 to 2.8 MPa) were obtained after activating WBA with a mixture of NaOH and sodium silicate (Na₂SiO₃) solutions, where curing time and temperature were 3 days and 75 °C, respectively [38,39]. Other studies obtained highly porous AACs after a long curing process of 20 months at room temperature [40]. The compressive strength was not reported in this case. It is important to highlight that there are no published studies where AACs (using WBA as the sole precursor) have been obtained by curing them under similar conditions of temperature (room temperature) and maximum curing time (28 days) to OPC. Low temperatures and curing times would improve the sustainability in the use of the AACs formulated using WBA as the sole precursor, facilitating their processing and increasing their applicability.

The main goal of this study is to evaluate the potential of new alkali-activated binders formulated with WBA as the sole precursor (AA-WBA). This research contributes to the development of new alternative cements and provides an added value to the WBA by-product. Different formulations were prepared using WBA as the sole precursor by mixing Na₂SiO₃ and different NaOH solutions for alkali activation. In contrast to the few similar research works found in the literature, the novelty and uniqueness of this study is based in the time and curing temperature, which facilitates

and increases the AA-WBA applicability. This work focuses on the effect of NaOH concentration from a physicochemical, physical, mechanical, and environmental point of view on the resultant binders.

2. Materials and Methods

The WBA sample was provided by the VECSA company, which is responsible for valorizing the IBA collected from the WtE plant located in Tarragona (Catalonia, Spain), with a capacity of 140 kt·y⁻¹. The feed stream treated in this incineration plant is mainly composed of household rubbish, with a small input from commercial sources. Around 32 kt·y⁻¹ of fresh IBA is obtained in this WtE plant. The combustion temperature is 950 °C [42]. After combustion, fresh IBA is further processed in a conditioning plant to recover some valuable materials (ferrous and non-ferrous metals) and to obtain a homogenized granular material. Finally, the resultant IBA is subjected to natural weathering outdoors for at least 3 months to stabilize heavy metal(loid)s and to obtain WBA, which is reused as secondary aggregate. Because of the heterogeneity of WBA, 100 kg were collected from stockpiles and then homogenized and stored in 30 L plastic containers. The alkali activator used consisted of a commercial Na₂SiO₃ solution (Scharlab S.L.; 26.44 wt.% of SiO₂ and 8.21 wt.% of Na₂O; $\rho = 1.37 \text{ g}\cdot\text{cm}^{-3}$) and NaOH solutions prepared by using NaOH pearls (Labbox Labware S.L.; purity > 98%) dissolved in distilled water: 2 ($\rho = 1.08 \text{ g}\cdot\text{cm}^{-3}$), 4 ($\rho = 1.16 \text{ g}\cdot\text{cm}^{-3}$), 6 ($\rho = 1.20 \text{ g}\cdot\text{cm}^{-3}$), and 8M ($\rho = 1.24 \text{ g}\cdot\text{cm}^{-3}$).

The preparation to obtain the WBA powder started by quartering the whole 100 kg sample to acquire a representative sub-sample of 10 kg. The quartered sample was dried in a stove at 105 °C for 24 h. Then, the dried sample was sieved (by using standard sieves: 32, 16, 8, 4, 2, 1, 0.5, 0.125, 0.063 mm) to determine the particle size distribution (PSD), as shown in Figure 1. Subsequently, the WBA was crushed and milled until a powder below 80 μm in particle size was obtained. Finally, a metal magnet (Nd; 0.485 T) was passed over the ground sample to remove magnetic particles.

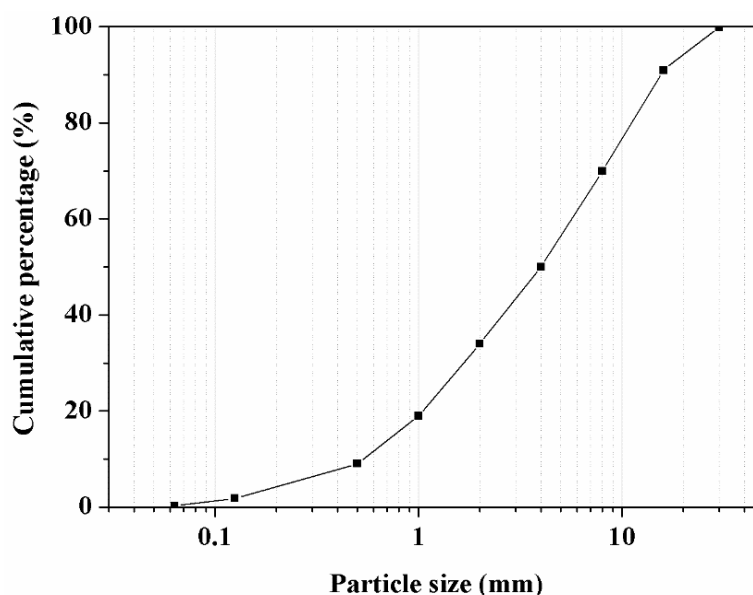


Figure 1. Particle size distribution of weathered bottom ash (WBA).

The elemental oxide composition of WBA was assessed by X-ray fluorescence (XRF) analysis with a spectrophotometer Panalytical Philips PW 2400 sequential X-ray equipped with the software UniQuant® V5.0. Major oxides are given in Table 1. There was a high content of SiO₂, CaO, Al₂O₃, and Na₂O, which are the main compounds used to obtain AACs [43]. The high SiO₂ content was due to the presence of primary and secondary glass in WBA [6,44]. The CaO and Al₂O₃ content was because WBA contains cementitious materials based on OPC, as well as synthetic ceramics from small domestic works. It is important to highlight that the percentage shown in Table 1 represents the total content of

the oxides considering both their amorphous and crystalline phases. The SiO₂ and Al₂O₃ availability (reactive phases) of the WBA sample are reported in previous studies by the authors [37].

Table 1. Elemental oxide composition of WBA powder.

Major Elements (wt.%)										
SiO ₂	CaO	Al ₂ O ₃	Na ₂ O	K ₂ O	Fe ₂ O ₃	MgO	TiO ₂	Cl ⁻	SO ₃	¹ LOI
45.44	17.55	10.38	5.04	1.54	6.08	2.66	0.65	1.42	2.57	5.78

¹ Loss on ignition at 1000 °C.

Figure 2 shows the WBA mineralogical results obtained by a Bragg–Brentano Siemens D-500 powder diffractometer device with CuK α radiation. A halo is observed between 20 and 35° due to the mainly vitreous nature of the WBA sample [6]. The main crystalline phases are rich in Si, Al, and Ca, such as quartz (SiO₂; PDF# 01-083-0539), calcite (CaCO₃; PDF# 01-072-1937), akermanite (Ca₂MgSi₂O₇; PDF# 01-076-0841), hydrocalumite (Ca₄Al₂(OH)12(Cl,CO₃,OH)₂·4H₂O; PDF# 016-0333), and pseudowollastonite (CaSiO₃; PDF# 01-074-0874). Muscovite (KAl₂(AlSi₃O₁₀)(OH)₂; PDF# 01-075-0948), microcline (KAlSi₃O₈; PDF# 01-076-0918), kyanite (Al₂SiO₅; PDF# 01-074-1827), and magnetite (Fe₃O₄; PDF# 01-077-1545) were also identified as minor crystalline phases.

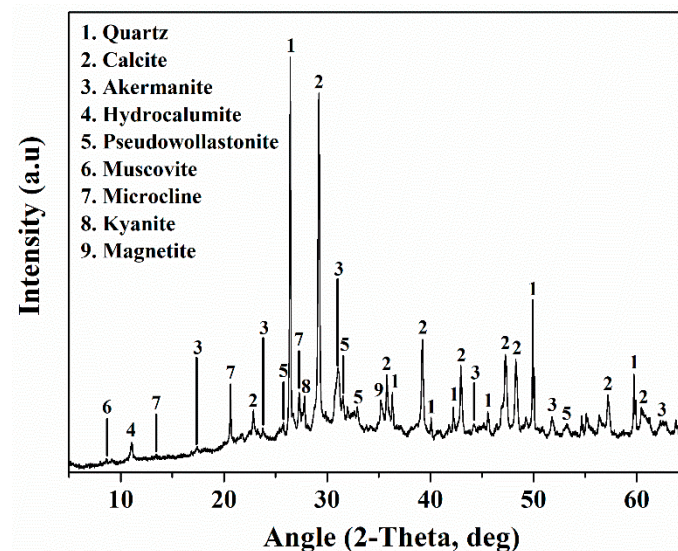


Figure 2. XRD pattern of WBA.

The proportions of the alkali-activator solution, alkali dosage, and silicate modulus (Ms) are given in Table 2. The formulation's optimal stoichiometry was determined after carrying out a preliminary study to delimit the proportion of raw materials and to obtain the best mechanical performance of AA-WBA binders cured at room temperature. The same amount of WBA, NaOH, and Na₂SiO₃ solutions (referred as liquid; L) were used in each formulation. The concentration of the NaOH solutions (2, 4, 6, and 8M) was varied to evaluate its effect on the AA-WBA final properties and structure of the cementitious matrix. The concentrations of NaOH were chosen considering the previous studies carried out by the authors [41].

Table 2. Alkali-activator solution proportions and chemical composition.

Reference	L				¹ Na ₂ SiO ₃ (wt.%)	¹ Na ₂ O (wt.%)	² SiO ₂ /Na ₂ O
	¹ NaOH (wt.%)						
	2M	4M	6M	8M			
AA-WBA-2M	20				80	7.7	3.6
AA-WBA-4M		20			80	8.7	3.2
AA-WBA-6M			20		80	9.7	2.9
AA-WBA-8M				20	80	10.7	2.6

¹ With respect to the WBA content. ² Molar ratio.

The AA-WBA binders' preparation procedure began by mixing the NaOH and Na₂SiO₃ (ratio of 1:4 by weight). This ratio was selected because a higher proportion of NaOH increases the porosity and reduces the mechanical performance of the binders [33]. Then, the WBA and the alkali-activator solution were mixed (liquid-to-solid ratio of 1:1 by weight) and mechanically stirred in a plastic beaker for 5 min. Fresh AA-WBA binders were poured into 25 mm cubic molds and sealed in plastic bags for 3 days in a climate chamber (25 ± 1 °C and relative humidity of 95% ± 5%). After 3 days, the samples were unmolded and removed from the plastic sealed bag, and the AA-WBA specimens continued curing in the climate chamber under the same above-mentioned conditions. Nine cubic-shaped specimens were prepared for each formulation. The AA-WBA specimens' characterization was carried out after 28 curing days.

The hydrolytic stability of the AA-WBA binders was evaluated by introducing a dried cubic specimen of each formulation in boiling water for 20 min [39]. Afterwards, the specimen remained at room temperature until reaching a constant weight in a desiccator with silica gel. Then, before and after the test, the sample was weighed to determine the mass loss and to verify the chemical stability and resistance to the dissolution of the AA-WBA binders. The integrity of AA-WBA was assessed by introducing a cubic specimen in deionized water (liquid-to-specimen ratio of 10.0 by weight) under stirring for 2 days. Conductivity (k) and pH were measured (after 1, 15, 30, 60, 120, 240, 600, 1440, 2160, and 2880 min) to evaluate pH variation and ion diffusion over time and the effect that may have on the formation of cementitious phases.

The main reaction product of alkali activation of calcium-rich precursors such as WBA [41] is calcium silicate hydrate (C-(A)-S-H) gel [39,45]. C-(A)-S-H gel coexists in the AAC's microstructures along with the N-A-S-H gel [46]. It has even been reported that a mixture of both gels improves the durability of AACs as compared to the single N-A-S-H gel [47]. However, when both formed gels coexist, it is difficult to conduct a proper elucidation of C-(A)-S-H using classical characterization techniques such as X-ray diffraction (XRD) or Fourier transform infrared spectroscopy (FTIR). For this reason, selective dissolution characterization is gaining popularity in order to eliminate any ambiguity between C-(A)-S-H and N-A-S-H gels [46]. AA-WBA binders were subjected to the salicylic acid/methanol (SAM) extraction [43] and HCl extraction [44] to determine C-(A)-S-H and N-A-S-H phases' content. The calcium-containing phases were dissolved in the SAM medium after the attack, while phases without calcium remained in the insoluble residue. The SAM extraction procedure consisted of mixing 1 g of grounded sample with salicylic acid (6 g) and methanol (40 mL) for 1 h. The mixture was subsequently filtered (Whatman filter with 20 µm pore size) to obtain the insoluble residue. The HCl extraction consisted of stirring 1 g of AA-WBA binder with 250 mL of HCl (1:20) solution for 3 h, followed by filtration (Whatman filter with 20 µm pore size). Then, the insoluble residues were washed with deionized water and dried in a desiccator until reaching a constant weight. The percentage of weight loss due to SAM and HCl extraction was calculated by weighing the insoluble residue.

XRD analysis was performed to determine the crystalline phases of AA-WBA binders. FTIR was used to determine the reaction products of alkali-activated WBA by means of various Si-O-X (X=Al, Si) stretching peaks' identification, which are assigned to different chemical structures of silicate

phases. Spectrum Two™ equipment from Perkin Elmer was used. The insoluble residue obtained in SAM and HCl extraction was also analyzed by FTIR to identify possible changes in the AA-WBA binders' composition and elucidate the co-existence of both C-(A)-S-H and N-A-S-H gels. A scanning electron microscopy (SEM) technique was conducted by an ESEM FEI Quanta 200 to evaluate the AA-WBA binders' microstructure. A planar sample (1.5 mm thickness) of each formulation was obtained by means of a diamond disc (140 rpm) cutter, and coated with graphite.

Bulk density and open porosity were studied by using 3 cubic shape specimens for each formulation. The values were determined following the standard EN 1936:2006. After 28 curing days of the AA-WBA specimens, compressive strength (σ_c) tests were performed using Incotecnic MULTI-R1 equipment. Three tests were performed for each formulation. A progressive load until fracture was applied with a loading rate of 240 kg·s⁻¹.

Leaching tests in deionized water for 24 h were conducted according to European standard EN 12457-2 to evaluate the potential release of heavy metal(loid)s from WBA and AA-WBA binders. A PerkinElmer ELAN 6000 ICP mass spectrometry (ICP-MS) device was used to analyze heavy metal(loid)s (As, Ba, Cd, Cr, Cu, Hg, Mo, Pb, Ni, Sb, and Zn) in the obtained eluates.

The cost of AA-WBA binders (€·t⁻¹) considering the cost of the raw materials (Table 3) used for their formulation was calculated.

Table 3. Raw materials cost (€·t⁻¹).

WBA	Na ₂ SiO ₃	NaOH (Pearls)	Water
0.6	566 [48]	884 [48]	1.9 [48]

3. Results and Discussion

3.1. Hydrolytic Stability Test and Integrity Test

The boiling water test demonstrated the AA-WBA binders' resistance to hydrolytic degradation. The specimen mass loss percentage was lower than 3% in all formulations. The AA-WBA binders also remain consolidated after the integrity test. Figure 3a shows the pH results of AA-WBA binders. There was a significant pH increase at the beginning of the integrity test due to the alkalinity of all samples. The pH values were stabilized after 120 min around a range between 10.75 and 11.25. The conductivity values (Figure 3b) increased gradually during the test because of the contribution of Na⁺ and OH⁻ ions found in unreacted NaOH and Na₂SiO₃. The presence of Cl⁻ ions in WBA also led to an increase of conductivity. As expected in both cases, the higher the concentration used to formulate the AA-WBA binder, the higher the pH and conductivity values obtained. These results demonstrate the chemical stability of AA-WBA binders.

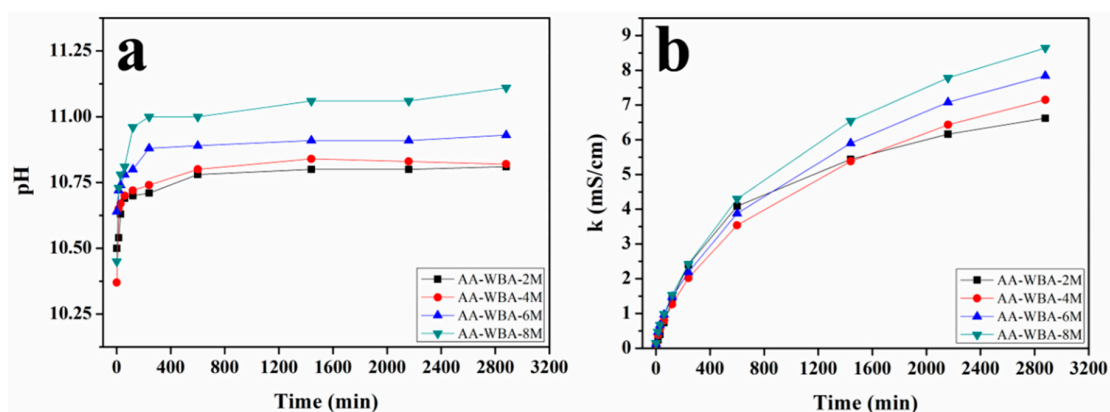


Figure 3. Alkali-activated weathered bottom ash binders' (AA-WBAs) values of (a) pH (b) conductivity during the integrity test.

3.2. Selective Chemical Extractions

The SAM and HCl extraction results are given in Table 4. The percentage of mass dissolved by SAM extraction in OPC paste compared with that of AA-WBA binders was higher due to its composition based in C-S-H phases. The main contribution of C-(A)-S-H phases dissolved in WBA powder probably came from the residues of small construction works in the domestic sphere. The most C-(A)-S-H formation in AA-WBA occurred in the AA-WBA-6M sample, as it showed the maximum value of dissolved mass by SAM extraction. A slight reduction of dissolved mass by SAM extraction in the AA-WBA-8M sample compared with that of the AA-WBA-6M sample was also observed. These results reveal that the NaOH 6M was the maximum NaOH concentration from which the precipitation of Ca^{2+} in form of C-(A)-S-H was disadvantaged against the formation of aluminosilicate gels [49]. The HCl extraction results show that increases in the NaOH concentration of AA-WBA binders resulted in an increase in the dissolved mass. The selective chemical extraction by HCl led to the dissolution of calcium and sodium carbonate phases [50], sodium aluminosilicate gels, and zeolites [44], as well as C-(A)-S-H phases leading to the removal of Ca^{2+} and leaving silica gel as an insoluble residue [46]. The results of HCl extraction indicate that the higher the NaOH concentration, the higher mass dissolved. This fact is due to the formation of C-A-S-H gels as demonstrated in SAM extraction, as well as the increased presence of sodium carbonate phases as the alkali dosage was increased (Table 2).

Table 4. Salicylic acid/methanol (SAM) and HCl extraction results.

	Mass Dissolved by SAM (wt.%)	Mass Dissolved by HCl (wt.%)
Portland cement paste	89.8	-
WBA powder	15.9	-
AA-WBA-2M	16.6	56.0
AA-WBA-4M	24.2	57.6
AA-WBA-6M	33.5	59.9
AA-WBA-8M	29.7	61.5

3.3. Physicochemical Characterization

The analysis of the XRD patterns of the WBA and AA-WBA binders shows the presence of new crystalline phases. The appearance of new peaks or variations demonstrates the formation of new crystalline phases in the AA-WBA binders. This can be observed in the shaded areas of Figure 4, where the XRD pattern of WBA compared with that of the AA-WBA-6M sample is shown.

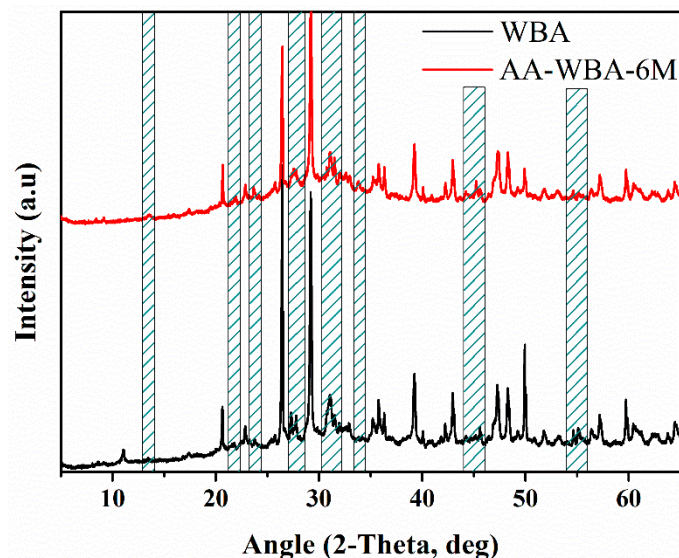


Figure 4. XRD patterns of WBA and AA-WBA-6M.

In the shaded areas of Figure 5a,b, some variation on the peaks' intensity between the AA-WBA binders is appreciated, therefore indicating that the amount of these new crystalline phases increases as the NaOH concentration increases.

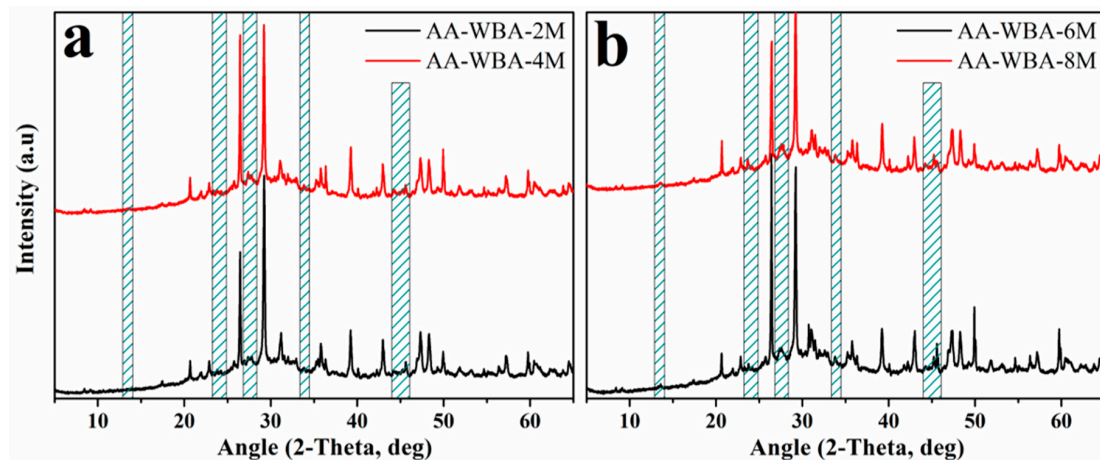


Figure 5. XRD patterns of (a) AA-WBA-2M and AA-WBA-4M, and (b) AA-WBA-6M and AA-WBA-8M.

Figure 6a,b depicts the XRD patterns of AA-WBA-6M and AA-WBA-8M samples, respectively. These two formulations contain the highest percentage of C-(A)-S-H phases as demonstrated above (see Section 3.2). In both cases, the main reaction products formed are calcium silicate hydrate (C-S-H; PDF# 003-0728), gehlenite ($\text{Ca}_2\text{Al}_2\text{SiO}_7$; PDF# 01-072-2128), and reinhardbraunsite ($\text{Ca}_5(\text{SiO}_4)_2(\text{OH})_2$; PDF# 029-0380). In the AA-WBA-8M sample, gismondine ($\text{CaAl}_2\text{Si}_2\text{O}_8 \cdot 4\text{H}_2\text{O}$; PDF# 020-0452) and gaylussite ($(\text{Na}_2\text{Ca}(\text{CO}_3)_2 \cdot 5\text{H}_2\text{O})$; PDF# 020-1088) were also identified. All the aforementioned compounds are related with C-(A)-S-H phases excluding gaylussite, which is a sodium carbonate compound that reveals the cation exchange between precursor and alkali-activator solution [51]. It is important to note that XRD results agree with the results obtained in the selective chemical extractions.

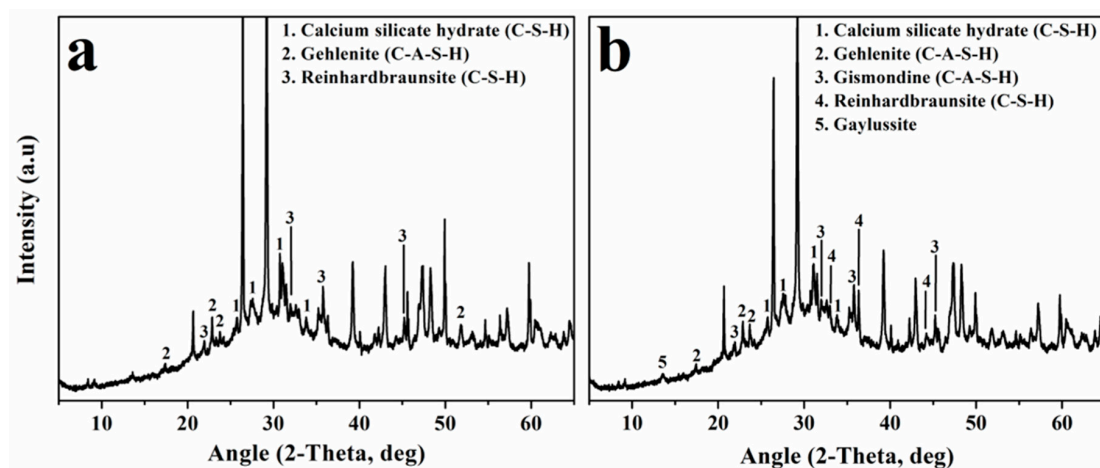


Figure 6. XRD patterns of (a) AA-WBA-6M and (b) AA-WBA-8M.

Depicted in Figure 7 is the WBA FTIR spectrum compared to the FTIR spectra of the AA-WBA binders, which was used to find evidence of the alkali-activation of the WBA. The broad band at 984 cm^{-1} ascribed to T-O stretching vibrations (where T=Si or Al) was displaced towards higher frequencies, indicating the formation of C-(A)-S-H gel [52]. With respect to the AA-WBA spectra, a shift of the main broad band towards lower frequencies was observed. This fact is probably due to both the inclusion of aluminum on the C-S-H gel [53], which is consistent with chemical extraction

and XRD results. There was a weak peak at 780 cm^{-1} associated with Si-O-Si bridging bonds in quartz (SiO_2) [54]. The peak mentioned above was indiscernible in AA-WBA-6M and AA-WBA-8M samples. This fact probably means that a large proportion of quartz had reacted to form new phases due to the higher alkalinity of the alkali-activator solution used. The strong band at 1429 cm^{-1} , assigned to the stretching mode of carbonates, as well as sharp peaks at 875 cm^{-1} and 713 cm^{-1} which were related to the bending mode of carbonates, were less intense in AA-WBA binders [54].

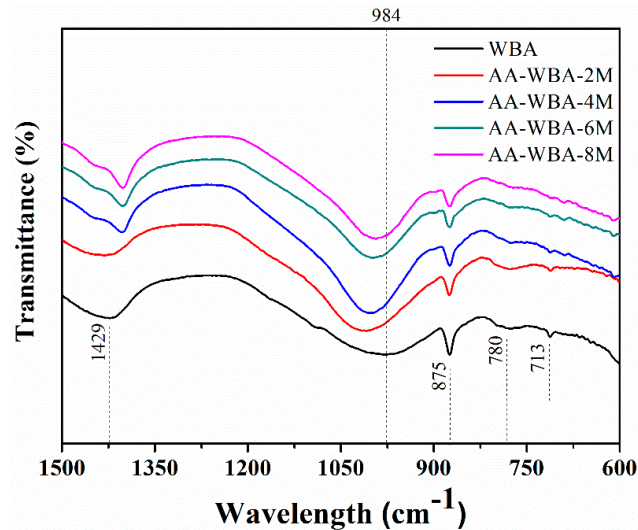


Figure 7. WBA and AA-WBA FTIR spectra.

The FTIR spectra of WBA before and after SAM is shown in Figure 8a. The band at 984 cm^{-1} associated with T-O stretching vibrations (where T=Si or Al) was shifted to 1003 cm^{-1} , which means that C-(A)-S-H phases were dissolved by SAM extraction [55]. The strong band at 1429 cm^{-1} , assigned to the stretching mode of carbonates, as well as sharp peaks at 875 cm^{-1} and 713 cm^{-1} related to the bending mode of carbonates, did not present any changes. Figure 8b shows the FTIR spectra of the AA-WBA-6M sample before and after SAM and HCl extraction. This sample was chosen because it was the one that would potentially present better results. A more pronounced shifting (995 to $\approx 1065\text{ cm}^{-1}$) in the band associated with T-O stretching vibrations (where T=Si or Al) could be observed because of the large amount of C-(A)-S-H phases in the AA-WBA-6M sample. Both in SAM extraction and HCl extraction spectra, three peaks (≈ 790 , ≈ 930 , $\approx 1050\text{ cm}^{-1}$) and a shoulder ($\approx 1162\text{ cm}^{-1}$) were also observed, which are characteristic of silica gels [56,57].

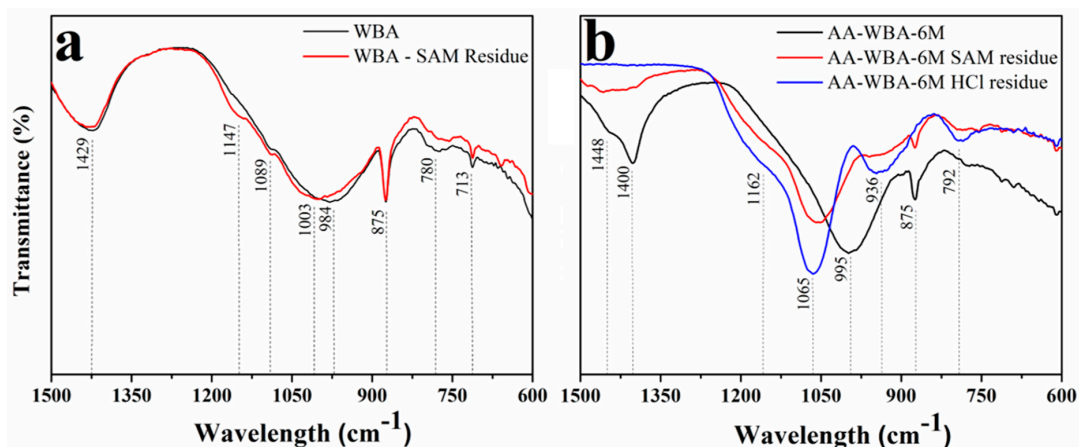


Figure 8. FTIR spectra before and after SAM extraction of (a) WBA and (b) AA-WBA-6M.

Figure 9 shows the SEM images of AA-WBA binders in backscattering electron (BSE) mode. The effect of alkali-activator concentration in the compactness and microstructure of the material is demonstrated. Two differentiated areas in all samples can be observed; a light grayish compact area which was essentially attributed to the C-(A)-S-H gel [52]; and a dark grayish disaggregated area composed of unreacted WBA. In the AA-WBA-2M sample (Figure 9a), it can be observed that the unreacted WBA area is prominent compared with the compact area. The same appearance on the AA-WBA-4M microstructure is shown in Figure 9b. However, there is a predominance of the C-(A)-S-H gel in the cement matrix in contrast with Figure 9a. The microstructure of the AA-WBA-6M (Figure 9c) shows a prominent lighter grayish homogeneous-colored matrix with two distinguished areas corresponding to C-(A)-S-H gel. The compact area is associated with the C-(A)-S-H gel formed by sodium silicate [52], while the rough compact area is ascribed to the C-(A)-S-H gel formed by NaOH [58]. The microstructure of AA-WBA-8M sample (Figure 9d) shows three distinguished areas: The same two light grayish areas of Figure 9c and a darker grayish area corresponding to the unreacted WBA. The formation of C-(A)-S-H gel to a greater or lesser extent, depending on NaOH in the alkali-activator solution used, was demonstrated. The SEM images reveals that the use of NaOH 6M led to a greater formation of the C-(A)-S-H gel in agreement with the selective extraction results mentioned above (Section 3.2).

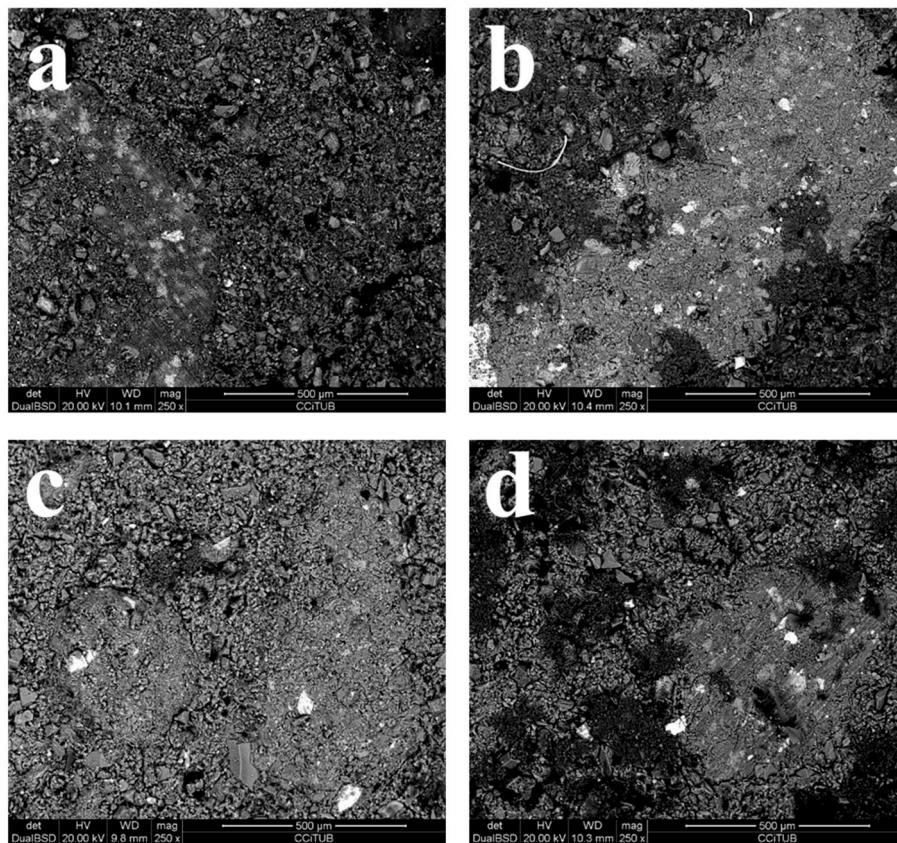


Figure 9. SEM images of AA-WBA binders. (a) 2, (b) 4, (c) 6, (d) 8M.

3.4. Physical and Mechanical Characterization

The density and open porosity of the AA-WBA binders were determined to analyze the mechanical behavior because these properties are extremely linked. The bulk density ($1.18 \pm 0.1 \text{ g}\cdot\text{cm}^{-3}$) and open porosity ($38 \pm 0.5\%$) results demonstrated the material formation with low density and porosity, probably due to the reaction between metallic aluminum and the alkaline activator to generate hydrogen gas [33,34]. Figure 10 depicts the compressive strength and bulk density results where the same trend can be observed in both cases. A maximum value of compressive strength and bulk

density was obtained in the AA-WBA-6M sample, in congruence with selective chemical extraction results and the AA-WBA microstructure observed in SEM images (Sections 3.2 and 3.3, respectively).

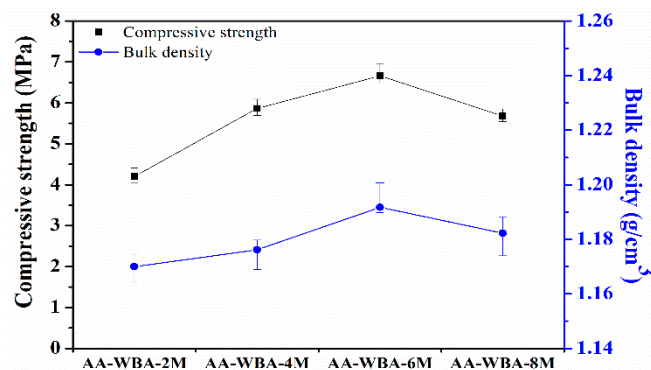


Figure 10. Bulk density and compressive strength of AA-WBA binders.

3.5. Environmental Characterization

The environmental characterization through leaching tests in deionized water according EN 12457-2 was performed to assess the potential release of heavy metal(loid)s in the AA-WBA binders. In the case of the WBA, the test was carried out for both a non-milled sample and milled sample to evaluate if the process of particle size reduction increased the potential release of heavy metals and metal(loid)s on leachates. In the AA-WBA, the test was carried out on crushed particles below 4 mm, aiming to simulate the worst possible scenario for the AA-WBA leachates, which is at the end of their life cycle when they are demolished. The leaching concentrations of heavy metal(loid)s in WBA and AA-WBA binders are given in Table 5. In WBA, the leaching concentrations of Cu, Cr (only for WBA powder), Mo, and Sb exceeded the limit for acceptance at landfills for inert waste [59]. Most of the heavy metal(loid)s were more leached (As, Pb, Ni, Sb, and Zn) in AA-WBA binders when compared to WBA due to pH increase and the greater pH-dependent metals’ mobility. Leaching concentration of Cu and Mo exceeded the acceptance at landfills for inert waste. However, Sb and As were the main causes of concern, since the former exceeded the limit marked for acceptance at landfills for non-hazardous waste, whilst As was very close to this limit. The presence of these two heavy metal(loid)s was because of the substantial amount of primary and secondary glass in the WBA [6]. Arsenic (As₂O₃) and antimony (Sb₂O₃) oxides are extensively used in the glass industry as fining agent, to lighten glass and to remove air bubbles [60]. It is important to highlight that the AA-WBA binders were subjected to an aggressive leaching test. The authors expect better results can be obtained with other, less aggressive leaching tests (such as the monolithic test). The environmental characterization reveals that the higher Na₂O content in alkali-activator solution, the higher the heavy metal(loid)s’ activation.

Table 5. Leaching concentrations (mg·kg⁻¹) on WBA and AA-WBA binders after leaching tests (EN 12457-2) and limits for acceptance at landfills.

Sample	As	Ba	Cd	Cr	Cu	Hg	Mo	Pb	Ni	Sb	Zn	pH
Non-milled WBA	0.02	0.42	<0.01	0.21	3.27	0.05	0.71	0.07	<0.03	0.23	0.90	9.66
WBA powder	0.04	0.37	<0.01	0.51	3.33	0.01	1.26	0.03	<0.03	0.35	0.44	11.33
AA-WBA-2M	1.29	0.05	0.01	0.47	3.46	<0.01	0.94	0.41	0.23	1.61	2.30	11.26
AA-WBA-4M	1.44	0.07	0.02	0.34	2.80	<0.01	0.85	0.51	0.27	1.50	3.26	11.39
AA-WBA-6M	1.51	0.08	0.00	0.27	3.25	0.01	0.88	0.54	0.29	1.62	3.44	11.62
AA-WBA-8M	1.65	0.08	0.00	0.37	3.91	0.12	0.89	0.40	0.12	1.93	3.09	11.77
¹ Inert waste (mg·kg ⁻¹)	0.5	20	0.04	0.5	2	0.01	0.5	0.5	0.4	0.06	4	
¹ Non-hazardous waste (mg·kg ⁻¹)	2	100	1	10	50	0.2	10	10	10	0.7	50	
¹ Hazardous waste (mg·kg ⁻¹)	25	300	5	70	100	2	30	50	40	5	200	

¹ Limit for acceptance at landfills [59].

3.6. AA-WBA Formulation Costs

The costs of AA-WBA formulations compared to OPC costs are shown in Table 6. An increase in the cost of AA-WBA binders in a range between 29 to 45% with respect to OPC can be observed. As expected, the higher the NaOH concentration, the higher the cost of the formulation due to the high cost of NaOH pearls. It is important to note that the electricity for the WBA grinding process was not considered; therefore, the formulation's final cost would be slightly higher. However, the key to produce a competitive AA-WBA binder in cost terms is to reduce the cost of sodium silicate.

Table 6. Cost ($\text{€}\cdot\text{t}^{-1}$ binder) of AA-WBA formulations.

OPC	AA-WBA-2M	AA-WBA-4M	AA-WBA-6M	AA-WBA-8M
106.2 [61]	137.6	143.3	148.8	153.9

4. Conclusions

The valorization of the WBA is a challenge to be solved by the WtE plants due to the continuous growth of MSW around the world. The work reported herein validates the potential of WBA as precursor in alkali-activated cements. The use of WBA as precursor promotes the zero-waste principle and contributes to the development of new low-carbon cements. Moreover, the novelty and uniqueness of this research was based on reducing the curing temperature of the AA-WBA. The curing at room temperature allowed for the extension and facilitation of the applicability of the AACs. The hydrolytic stability and integrity tests demonstrated that AA-WBA were properly bonded. Selective chemical extraction and physicochemical characterization revealed the formation of C-(A)-S-H gel in the AA-WBA. It also proved the influence of the alkali-activator concentration in their microstructure. The selective chemical extraction and physical characterization results were in accordance with the compressive strength results, where it was demonstrated that the use of AA-WBA is only for non-structural purposes. Environmental characterization showed a concerning activation of As and Sb, which entails a setback for the waste management of the material once its cycle of life is finalized. The cost of the AA-WBA formulations demonstrate that it is not possible to compete with OPC in economic terms due to the high cost of sodium silicate. It would be necessary to search alternatives to produce a sodium silicate from waste glass, making AA-WBA binders more economical and sustainable.

The authors will focus their future line investigation on the formulation of AA-WBA using the least polluted fractions of WBA (coarser fractions). The main aim is using fractions that contain greater availability of SiO_2 , hence favoring the formation of C-(A)-S-H and N-A-S-H gels to enhance the mechanical properties of AA-WBA. The environmental properties of AA-WBA binders would also improve given the low content of heavy metal(loid)s in coarse fractions.

Author Contributions: Conceptualization, J.M.C. and J.G.-P.; methodology, À.M.-A. and A.A.-R.; validation, J.G.-P., J.F., and J.M.C.; formal analysis, À.M.-A.; investigation, À.M.-A. and A.A.-R.; data curation, J.F.; writing—original draft preparation, À.M.-A.; writing—review and editing, J.G.-P., J.F., and J.M.C.; supervision, J.M.C. and J.G.-P.; funding acquisition, J.M.C. All authors have read and agreed to the published version of the manuscript.

Funding: This research was funded by the Spanish Government (BIA2017-83912-C2-1-R).

Acknowledgments: The authors would like to thank the Catalan Government for the quality accreditation given to their research groups DIOPMA (2017 SGR 118). The authors also want to thank SIRUSA and VECSA for supplying MSWI Bottom Ash and Karla Montes for the linguistic revision. Alex Maldonado–Alameda is grateful to the Government of Catalonia for the research Grant (FI-DGR 2017).

Conflicts of Interest: The authors declare that they have no known competing financial interests or personal relationships that could have appeared to influence the work reported in this paper.

References

1. European Commission. *The Role of Waste-to-Energy in the Circular Economy*; European Commission: Brussels, Belgium, 2017; Available online: http://ec.europa.eu/priorities/energy-union-and-climate/state-energy-union_en%0Ahttp://ec.europa.eu/environment/waste/waste-to-energy.pdf (accessed on 11 June 2020).
2. Cheng, H.; Hu, Y. Municipal solid waste (MSW) as a renewable source of energy: Current and future practices in China. *Bioresour. Technol.* **2010**, *101*, 3816–3824. [[CrossRef](#)] [[PubMed](#)]
3. Confederation of European Waste-to-Energy Plants. *Waste-to-Energy Plants in Europe in 2017*; CEWEP: Brussels, Belgium, 2019; Available online: <https://www.cewep.eu/waste-to-energy-plants-in-europe-in-2017/> (accessed on 11 June 2020).
4. Bontempi, E.; Šyc, M.; Lederer, J.; Quina, M.J.; Blanc-Biscarat, D.; Bogush, A.; Bontempi, E.; Blondeau, J.; Chimenos, J.M.; Quina, M.J.; et al. Legal situation and current practice of waste incineration bottom ash utilisation in Europe. *Waste Manag.* **2020**, *102*, 868–883. [[CrossRef](#)]
5. Eurostat—European Statistical Office. *Municipal Waste Statistics*, Luxembourg. 2019. Available online: https://ec.europa.eu/eurostat/statistics-explained/index.php?title=Municipal_waste_statistics (accessed on 11 June 2020).
6. Del Valle-Zermeño, R.; Gómez-Manrique, J.; Paloma, J.G.; Formosa, J.; Simon, F.-G. Material characterization of the MSWI bottom ash as a function of particle size. Effects of glass recycling over time. *Sci. Total Environ.* **2017**, *581*, 897–905. [[CrossRef](#)] [[PubMed](#)]
7. Wei, Y.; Shimaoka, T.; Saffarzadeh, A.; Takahashi, F. Mineralogical characterization of municipal solid waste incineration bottom ash with an emphasis on heavy metal-bearing phases. *J. Hazard. Mater.* **2011**, *187*, 534–543. [[CrossRef](#)] [[PubMed](#)]
8. Chimenos, J.M.; Fernandez, A.I.; Nadal, R.; Espiell, F. Short-term natural weathering of MSWI bottom ash. *J. Hazard. Mater.* **2000**, *79*, 287–299. [[CrossRef](#)]
9. Verbinnen, B.; Billen, P.; Van Caneghem, J.; Vandecasteele, C. Recycling of MSWI Bottom Ash: A Review of Chemical Barriers, Engineering Applications and Treatment Technologies. *Waste Biomass Valoriz.* **2016**, *8*, 1453–1466. [[CrossRef](#)]
10. Silva, R.; De Brito, J.; Lynn, C.; Dhir, R.K. Use of municipal solid waste incineration bottom ashes in alkali-activated materials, ceramics and granular applications: A review. *Waste Manag.* **2017**, *68*, 207–220. [[CrossRef](#)]
11. Shi, C.; Fernandez-Jiménez, A.; Palomo, A. New cements for the 21st century: The pursuit of an alternative to Portland cement. *Cem. Concr. Res.* **2011**, *41*, 750–763. [[CrossRef](#)]
12. Provis, J.L.; Palomo, A.; Shi, C. Advances in understanding alkali-activated materials. *Cem. Concr. Res.* **2015**, *78*, 110–125. [[CrossRef](#)]
13. Duxson, P.; Fernandez-Jiménez, A.; Provis, J.L.; Lukey, G.C.; Palomo, A.; Van Deventer, J.S.J. Geopolymer technology: The current state of the art. *J. Mater. Sci.* **2006**, *42*, 2917–2933. [[CrossRef](#)]
14. Lodeiro, I.G.; Palomo, A.; Fernandez-Jiménez, A.; Macphee, D. Compatibility studies between N-A-S-H and C-A-S-H gels. Study in the ternary diagram Na₂O–CaO–Al₂O₃–SiO₂–H₂O. *Cem. Concr. Res.* **2011**, *41*, 923–931. [[CrossRef](#)]
15. Fernandez-Jiménez, A.; Palomo, A. Composition and microstructure of alkali activated fly ash binder: Effect of the activator. *Cem. Concr. Res.* **2005**, *35*, 1984–1992. [[CrossRef](#)]
16. De Vargas, A.S.; Molin, D.C.D.; Vilela, A.; Da Silva, F.J.; Pavão, B.; Veit, H.M. The effects of Na₂O/SiO₂ molar ratio, curing temperature and age on compressive strength, morphology and microstructure of alkali-activated fly ash-based geopolymers. *Cem. Concr. Compos.* **2011**, *33*, 653–660. [[CrossRef](#)]
17. Alonso, S.; Vázquez, T.; Puertas, F.; Martínez-Ramírez, S. Alkali-activated fly ash/slag cement Strength behaviour and hydration products. *Cem. Concr. Res.* **2000**, *30*, 1625–1632.
18. Bakharev, T. Resistance of geopolymer materials to acid attack. *Cem. Concr. Res.* **2005**, *35*, 658–670. [[CrossRef](#)]
19. Provis, J.L.; van Deventer, J.S.J. *Geopolymers: Structures, Processing, Properties and Industrial Applications*; Elsevier: Amsterdam, The Netherlands, 2009.
20. Van Deventer, J.S.J.; Provis, J.L.; Duxson, P. Technical and commercial progress in the adoption of geopolymer cement. *Miner. Eng.* **2012**, *29*, 89–104. [[CrossRef](#)]

21. Bernal, S.A.; Rodriguez, E.D.; Kirchheim, A.P.; Provis, J.L. Management and valorisation of wastes through use in producing alkali-activated cement materials. *J. Chem. Technol. Biotechnol.* **2016**, *91*, 2365–2388. [CrossRef]
22. Rivera, J.; Castro, F.; Fernández-Jiménez, A.; Cristelo, N. Alkali-Activated Cements from Urban, Mining and Agro-Industrial Waste: State-of-the-art and Opportunities. *Waste Biomass Valoriz.* **2020**. [CrossRef]
23. Provis, J.L. Alkali-activated materials. *Cem. Concr. Res.* **2018**, *114*, 40–48. [CrossRef]
24. Lancellotti, I.; Kamseu, E.; Michelazzi, M.; Barbieri, L.; Corradi, A.; Leonelli, C. Chemical stability of geopolymers containing municipal solid waste incinerator fly ash. *Waste Manag.* **2010**, *30*, 673–679. [CrossRef]
25. Galiano, Y.L.; Pereira, C.F.; Vale, J. Stabilization/solidification of a municipal solid waste incineration residue using fly ash-based geopolymers. *J. Hazard. Mater.* **2011**, *185*, 373–381. [CrossRef]
26. Zhong, L.; Wang, C.; Wang, W.; Shi, Y.; Gao, X. Immobilization of MSWI fly ash through geopolymerization: Effects of water-wash. *Waste Manag.* **2011**, *31*, 311–317. [CrossRef] [PubMed]
27. Komnitsas, K. Potential of geopolymer technology towards green buildings and sustainable cities. *Procedia Eng.* **2011**, *21*, 1023–1032. [CrossRef]
28. European Commission. *Towards a Circular Economy: A Zero Waste Programme for Europe*; European Commission: Brussels, Belgium, 2014; Available online: https://eur-lex.europa.eu/resource.html?uri=cellar:aa88c66d-4553-11e4-a0cb-01aa75ed71a1.0022.03/DOC_1&format=PDF (accessed on 11 June 2020).
29. Lancellotti, I.; Ponzoni, C.; Barbieri, L.; Leonelli, C. Alkali activation processes for incinerator residues management. *Waste Manag.* **2013**, *33*, 1740–1749. [CrossRef] [PubMed]
30. Lodeiro, I.G.; Carcelen-Taboada, V.; Fernandez-Jiménez, A.; Palomo, A. Manufacture of hybrid cements with fly ash and bottom ash from a municipal solid waste incinerator. *Constr. Build. Mater.* **2016**, *105*, 218–226. [CrossRef]
31. Huang, G.; Ji, Y.; Li, J.; Zhang, L.; Liu, X.; Liu, B. Effect of activated silica on polymerization mechanism and strength development of MSWI bottom ash alkali-activated mortars. *Constr. Build. Mater.* **2019**, *201*, 90–99. [CrossRef]
32. Lancellotti, I.; Ponzoni, C.; Bignozzi, M.C.; Barbieri, L.; Leonelli, C. Incinerator Bottom Ash and Ladle Slag for Geopolymers Preparation. *Waste Biomass Valorization* **2014**, *5*, 393–401. [CrossRef]
33. Saffarzadeh, A.; Arumugam, N.; Shimaoka, T. Aluminum and aluminum alloys in municipal solid waste incineration (MSWI) bottom ash: A potential source for the production of hydrogen gas. *Int. J. Hydrog. Energy* **2016**, *41*, 820–831. [CrossRef]
34. Zhu, W.; Rao, X.H.; Liu, Y.; Yang, E.-H. Lightweight aerated metakaolin-based geopolymer incorporating municipal solid waste incineration bottom ash as gas-forming agent. *J. Clean. Prod.* **2018**, *177*, 775–781. [CrossRef]
35. Huang, G.; Yuan, L.; Ji, Y.; Liu, B.; Xu, Z. Cooperative action and compatibility between Portland cement and MSWI bottom ash alkali-activated double gel system materials. *Constr. Build. Mater.* **2019**, *209*, 445–453. [CrossRef]
36. Liu, Y.; Sidhu, K.S.; Chen, Z.; Yang, E.-H. Alkali-treated incineration bottom ash as supplementary cementitious materials. *Constr. Build. Mater.* **2018**, *179*, 371–378. [CrossRef]
37. Chen, Z.; Yang, E.-H. Early age hydration of blended cement with different size fractions of municipal solid waste incineration bottom ash. *Constr. Build. Mater.* **2017**, *156*, 880–890. [CrossRef]
38. Chen, Z.; Liu, Y.; Zhu, W.; Yang, E.-H. Incinerator bottom ash (IBA) aerated geopolymer. *Constr. Build. Mater.* **2016**, *112*, 1025–1031. [CrossRef]
39. Zhu, W.; Chen, X.; Struble, L.J.; Yang, E.-H. Characterization of calcium-containing phases in alkali-activated municipal solid waste incineration bottom ash binder through chemical extraction and deconvoluted Fourier transform infrared spectra. *J. Clean. Prod.* **2018**, *192*, 782–789. [CrossRef]
40. Lancellotti, I.; Cannio, M.; Bollino, F.; Catauro, M.; Barbieri, L.; Leonelli, C. Geopolymers: An option for the valorization of incinerator bottom ash derived “end of waste”. *Ceram. Int.* **2015**, *41*, 2116–2123. [CrossRef]
41. Maldonado-Alameda, A.; Paloma, J.G.; Svobodova-Sedlackova, A.; Formosa, J.; Simon, F.-G. Municipal solid waste incineration bottom ash as alkali-activated cement precursor depending on particle size. *J. Clean. Prod.* **2020**, *242*, 118443. [CrossRef]
42. Chimenos, J.M.; Segarra, M.; Fernández, M.; Espiell, F. Characterization of the bottom ash in municipal solid waste incinerator. *J. Hazard. Mater.* **1999**, *64*, 211–222. [CrossRef]

43. Lodeiro, I.G.; Macphee, D.E.; Palomo, A.; Fernández-jiménez, A. Effect of alkalis on fresh C–S–H gels. FTIR analysis. *Cem. Concr. Res.* **2009**, *39*, 147–153. [[CrossRef](#)]
44. Fernandez-Jiménez, A.; Palomo, A. Mid-infrared spectroscopic studies of alkali-activated fly ash structure. *Microporous Mesoporous Mater.* **2005**, *86*, 207–214. [[CrossRef](#)]
45. Huang, G.; Ji, Y.; Zhang, L.L.; Li, J.; Hou, Z. The influence of curing methods on the strength of MSWI bottom ash-based alkali-activated mortars: The role of leaching of OH[−] and free alkali. *Constr. Build. Mater.* **2018**, *186*, 978–985. [[CrossRef](#)]
46. Puligilla, S.; Mondal, P. Co-existence of aluminosilicate and calcium silicate gel characterized through selective dissolution and FTIR spectral subtraction. *Cem. Concr. Res.* **2015**, *70*, 39–49. [[CrossRef](#)]
47. Zhuang, X.Y.; Chen, L.; Komarneni, S.; Zhou, C.; Tong, D.S.; Yang, H.M.; Yu, W.H.; Wang, H. Fly ash-based geopolymer: Clean production, properties and applications. *J. Clean. Prod.* **2016**, *125*, 253–267. [[CrossRef](#)]
48. You, S.; Ho, S.W.; Li, T.; Maneerung, T.; Wang, C.-H. Techno-economic analysis of geopolymer production from the coal fly ash with high iron oxide and calcium oxide contents. *J. Hazard. Mater.* **2019**, *361*, 237–244. [[CrossRef](#)] [[PubMed](#)]
49. Alonso, S.; Palomo, A. Calorimetric study of alkaline activation of calcium hydroxide–metakaolin solid mixtures. *Cem. Concr. Res.* **2001**, *31*, 25–30. [[CrossRef](#)]
50. Taylor, H. Cement chemistry. *Cem. Chem.* **1997**. [[CrossRef](#)]
51. Kovtun, M.; Kearsley, E.; Shekhovtsova, J. Chemical acceleration of a neutral granulated blast-furnace slag activated by sodium carbonate. *Cem. Concr. Res.* **2015**, *72*, 1–9. [[CrossRef](#)]
52. Puertas, F.; Fernández-Jiménez, A.; Blanco-Varela, M.T. Pore solution in alkali-activated slag cement pastes. Relation to the composition and structure of calcium silicate hydrate. *Cem. Concr. Res.* **2004**, *34*, 139–148. [[CrossRef](#)]
53. Walkley, B.; Nicolas, R.S.; Sani, M.-A.; Rees, G.J.; Hanna, J.V.; Van Deventer, J.S.J.; Provis, J.L. Phase evolution of C-(N)-A-S-H/N-A-S-H gel blends investigated via alkali-activation of synthetic calcium aluminosilicate precursors. *Cem. Concr. Res.* **2016**, *89*, 120–135. [[CrossRef](#)]
54. Criado, M.; Palomo, A.; Fernandez-Jiménez, A. Alkali activation of fly ashes. Part 1: Effect of curing conditions on the carbonation of the reaction products. *Fuel* **2005**, *84*, 2048–2054. [[CrossRef](#)]
55. Ravikumar, D.; Neithalath, N. Effects of activator characteristics on the reaction product formation in slag binders activated using alkali silicate powder and NaOH. *Cem. Concr. Compos.* **2012**, *34*, 809–818. [[CrossRef](#)]
56. Lodeiro, I.G.; Fernandez-Jiménez, A.; Blanco, M.T.; Palomo, A. FTIR study of the sol–gel synthesis of cementitious gels: C–S–H and N–A–S–H. *J. Sol Gel Sci. Technol.* **2007**, *45*, 63–72. [[CrossRef](#)]
57. Zhu, W.; Chen, X.; Zhao, A.; Struble, L.J.; Yang, E.-H. Synthesis of high strength binders from alkali activation of glass materials from municipal solid waste incineration bottom ash. *J. Clean. Prod.* **2019**, *212*, 261–269. [[CrossRef](#)]
58. Puertas, F.; Palacios, M.; Manzano, H.; Dolado, J.S.; Rico, A.; Rodriguez, J. A model for the C-A-S-H gel formed in alkali-activated slag cements. *J. Eur. Ceram. Soc.* **2011**, *31*, 2043–2056. [[CrossRef](#)]
59. Council of the European Union. 2003/33/EC, Council Decision establishing criteria and procedures for the acceptance of waste at landfills pursuant to Article 16 of and Annex II to Directive 1999/31/EC. *Off. J. Eur. Communities* **2003**, *11*, 27–49.
60. Apostoli, P.; Giusti, S.; Bartoli, D.; Perico, A.; Bavazzano, P.; Alessio, L. Multiple exposure to arsenic, antimony, and other elements in art glass manufacturing. *Am. J. Ind. Med.* **1998**, *34*, 65–72. [[CrossRef](#)]
61. McLellan, B.; Williams, R.; Lay, J.; Van Riessen, A.; Corder, G. Costs and carbon emissions for geopolymer pastes in comparison to ordinary portland cement. *J. Clean. Prod.* **2011**, *19*, 1080–1090. [[CrossRef](#)]

